Tropical Aquatic and Soil Pollution

Research Article
Volume 6(1), 2026, 40−53
https://doi.org/10.53623/tasp.v6i1.1067

Phytoremediation of Coal Mine Acid Drainage Using the Invasive Weed *Cyperus rotundus* and *Typha angustifolia*: Optimizing Biomass Density in a Substrate-Free Batch System

Rinda Rahmadhani, Muhammad Mahfuzh Huda*, Rabiatul Adawiyah, Jevon Ona Ivena

Department of Environmental Engineering Universitas Muhammadiyah Berau, Tanjung Redeb, Indonesia

*Correspondence: hudamahfuzh@gmail.com

SUBMITTED: 22 February 2026; REVISED: 24 May 2026; ACCEPTED: 26 May 2026

ABSTRACT: Acid mine drainage (AMD) presents a persistent environmental challenge, particularly in tropical mining regions. This study evaluated the phytoremediation potential of the zero-cost invasive weed *Cyperus rotundus* against the established hyperaccumulator *Typha angustifolia* in a substrate-free batch system. Utilizing extreme raw AMD (pH 2.69; Fe 6.40 ppm; TDS 1,390 ppm), the experiment encompassed a baseline comparison (9 clumps), density optimization (6–15 clumps), and a synergistic mixed-culture evaluation over 15 days. Baseline results indicated that *T. angustifolia* intrinsically outperformed *C. rotundus* in iron (Fe) removal (89.10% vs. 82.22%) by day 10. However, optimizing *C. rotundus* to a 15-clump saturation threshold successfully overcame this deficit, achieving 91.20% Fe attenuation (0.56 ppm). Crucially, extended hydraulic retention (15 days) in high-density configurations induced a severe secondary pollution event, catastrophically increasing Total Dissolved Solids (TDS) to 2,300 ppm because of biomass carrying capacity limits and necrosis. The mixed-culture configuration exhibited the highest overall efficacy, maximizing Fe removal (92.63%), buffering pH to 3.27, and moderating late-stage TDS spikes. The findings demonstrated that while *C. rotundus* was a highly viable bioremediator, engineering designs needed to cap biomass at the saturation threshold and strictly enforce a 6- to 10-day retention window to prevent secondary decay pollution.

KEYWORDS: Acid mine drainage; phytoremediation; *Cyperus rotundus*; *Typha angustifolia*; ion removal

1. Introduction

Acid mine drainage (AMD) remained one of the most persistent environmental legacies of coal mining, characterized by low pH and elevated concentrations of dissolved metals that can severely degrade receiving waters and aquatic ecosystems [1, 2]. In tropical mining hubs such as East Kalimantan, Indonesia, the widespread use of open-pit extraction methods drastically exacerbated this issue, exposing vast quantities of sulfide-bearing rock to high atmospheric

oxygen and intense rainfall. The resulting AMD frequently threatened critical local watersheds, which served as primary raw water sources. Conventional AMD treatment technologies, particularly active chemical neutralization, were effective but often entailed high operational and maintenance costs, continuous chemical inputs, and intensive operational control [3,4]. These constraints limited their long-term feasibility, especially in developing regions and for unmanaged or abandoned mining sites. Consequently, there was increasing interest in passive and nature-based treatment approaches that relied on biogeochemical processes to attenuate acidity and metal loads with lower energy and operational demands [6].

Among passive technologies, aquatic phytoremediation had attracted considerable attention as a relatively low-cost and environmentally compatible option for AMD management [6, 7]. Aquatic macrophytes could facilitate metal removal directly through rhizofiltration, sorption to root surfaces (such as iron plaque formation), and stimulation of microbially mediated precipitation in the root zone [8–10].

Previous studies had reported variable removal efficiencies depending on plant species, hydraulic retention time, and biomass density [11–13]. However, the majority of published work had heavily relied on a limited set of established hyperaccumulators (e.g., *Typha* spp., *Phragmites* spp.), while the bioremediation potential of highly resilient, locally abundant tropical weeds remained comparatively underexplored [14]. Specifically, *Cyperus rotundus*—an aggressive, highly adaptable invasive sedge ubiquitous in tropical regions—presented a unique opportunity. Utilizing such species could transform a pervasive agricultural nuisance into a "zero-cost" bioremediator. Addressing this knowledge gap was critical for developing context-specific, highly scalable treatment systems that could be readily implemented in remote tropical mining regions.

In current phytoremediation practice, *Typha angustifolia* was a well-documented hyperaccumulator frequently employed in conventional constructed wetlands for metal-laden effluent treatment [12, 16]. Conversely, *Cyperus rotundus* was widely recognized as a noxious invasive agricultural weed characterized by aggressive vegetative propagation [17]. Recent empirical investigations demonstrated that these resilient botanical traits translated into highly effective bioremediation capabilities. Field evaluations conducted in heavily polluted aquatic environments showed that *C. rotundus* exhibited a strong natural capacity for heavy metal uptake, particularly iron (Fe), which accumulated predominantly in its dense fibrous root system [17]. Furthermore, controlled heavy metal stress trials confirmed its role as an effective phytostabilizer [18, 19]. Mathematical uptake indices revealed that *C. rotundus* sequestered toxic metals largely within its below-ground biomass, demonstrating a bioaccumulation factor (BCF) > 1 and a translocation factor (TF) < 1 [18, 19].

This empirical tendency for below-ground stabilization aligned well with the rhizospheric iron plaque formation mechanism targeted in the present substrate-free system. However, comparative evaluations of these two species, particularly in substrate-free, batch-operated configurations designed to isolate root-mediated metal removal, remained limited. Furthermore, the interactive effects of biomass density and hydraulic retention time on AMD quality improvement, particularly the balance between Fe removal and secondary pollution from biomass decay, had not been systematically quantified for tropical systems [11, 13, 17]. This represented a critical knowledge gap, as defining operational thresholds was essential for optimizing passive treatment design and scale-up. To address this gap while mitigating ecological risks associated with its invasive nature, *C. rotundus* was strictly confined within

controlled batch reactors, preventing rhizome spread while enabling controlled utilization of its phytoremediation potential.

In contrast, *T. angustifolia* was a well-established hyperaccumulator widely used in constructed wetland systems for metal-laden effluent treatment [12,16]. Comparative evaluations of both species in substrate-free batch systems remained limited. Additionally, the influence of biomass density and hydraulic retention time on AMD treatment performance, particularly in relation to Fe removal efficiency and TDS rebound from biomass decay, had not been systematically evaluated [11, 13, 17]. This represented a significant gap in understanding for tropical AMD treatment systems.

Therefore, the present study aimed to assess the phytoremediation performance of *C. rotundus* and *T. angustifolia* in a laboratory-scale, substrate-free batch system treating highly acidic AMD from a coal mining area in East Kalimantan, Indonesia. Specifically, this study: (i) compared Fe removal and pH buffering performance between monoculture and mixed-culture systems; (ii) evaluated the effects of biomass density (6, 9, 12, and 15 clumps) and hydraulic retention time (0–15 days) on water quality dynamics; and (iii) identified critical operational thresholds to maximize metal removal while minimizing secondary pollution (TDS spikes) from biomass decay. By elucidating both performance potential and saturation limits of locally abundant macrophytes, this study provided empirical evidence to optimize zero-cost, nature-based AMD treatment systems [6, 11, 14].

2. Materials and Methods

2.1. AMD sampling and characterization

AMD was collected from an active coal mining area in Berau Regency, East Kalimantan, Indonesia. The sampling location represented typical AMD generated from open-pit coal mining under tropical climatic conditions [18]. Grab samples were collected in polyethylene containers following standard water sampling procedures, transported to the laboratory under cooled conditions, and stored at 4°C prior to experimentation to minimize physicochemical changes [19]. Initial AMD characteristics were determined following standard water quality assessment protocols [20] to establish baseline conditions. The raw AMD exhibited extreme characteristics that exceeded local discharge thresholds, with a highly acidic pH of 2.69, Total Dissolved Solids (TDS) of 1,390 ppm, and dissolved iron (Fe) concentration of 6.40 ppm.

2.2. Phytoremediation system design.

A laboratory-scale, batch-operated Free Water Surface (FWS) reactor system was used to simulate passive AMD treatment under controlled conditions, consistent with modified constructed wetland systems for mine water remediation [7, 16]. Each reactor consisted of a plastic container (approximately 49 cm × 34 cm × 30 cm) operated as a strictly substrate-free system. To isolate plant-mediated remediation from substrate filtration effects, macrophytes were placed directly in the AMD solution without gravel or sand media [8, 10]. The system was operated under static batch conditions, where a fixed volume of AMD was introduced and retained without inflow or outflow. This design enabled controlled evaluation of hydraulic retention time effects and temporal remediation dynamics over a 15-day period, consistent with established laboratory wetland methodologies [11, 21], as illustrated in Figure 1, which shows

the experimental configuration of the batch-operated Free Water Surface (FWS) reactor system.

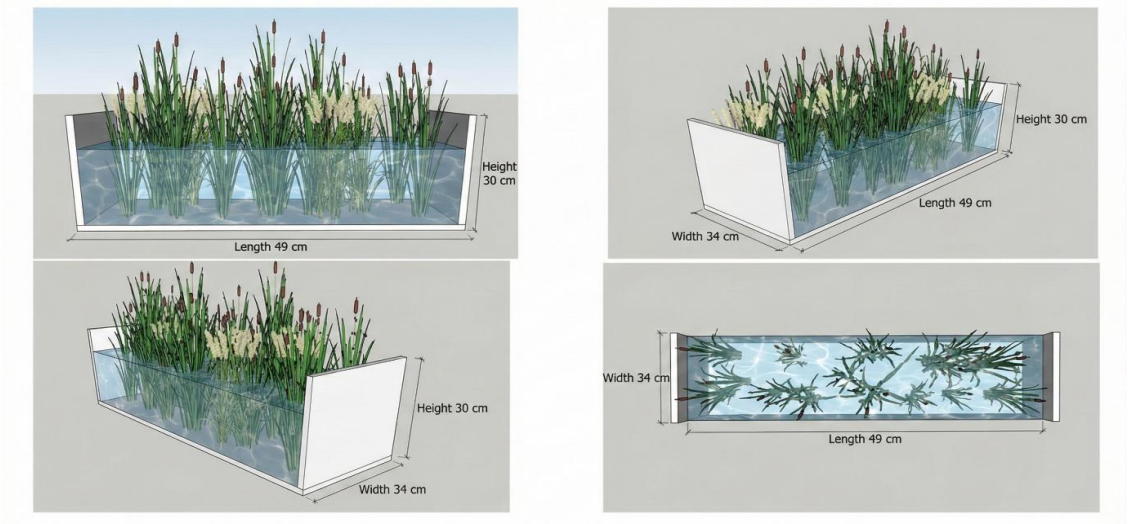

Figure 1. Illustration for experimental design using batch-operated Free Water Surface (FWS) reactor system.

2.3. Plant material and acclimatization.

Two macrophyte species were utilized: the highly adaptable invasive sedge *Cyperus rotundus* and the established wetland plant *Typha angustifolia*. Healthy, morphologically uniform specimens were collected locally from Berau Regency. To minimize transplant shock and induce physiological tolerance to the extreme baseline conditions of raw AMD, the plants were subjected to a rigorous 14-day acclimatization period prior to experimentation [12, 22]. This adaptation phase was conducted using a stepwise exposure protocol, gradually increasing the volumetric proportion of AMD relative to freshwater, culminating in 100% raw AMD exposure by the end of the second week [23]. Only specimens that exhibited robust vegetative health and no visible stress symptoms, such as chlorosis or wilting, after this 14-day period were selected for the experimental reactors to ensure baseline consistency and reliable treatment performance [15].

2.4. Experimental design.

The experimental setup was strategically designed in distinct phases to systematically evaluate intrinsic phytoremediation capacity followed by biological optimization. The substrate-free batch reactors were operated over a 15-day period. Initially, to establish an equitable baseline of intrinsic remediation efficiency, monocultures of both the established hyperaccumulator *T. angustifolia* and the invasive weed *C. rotundus* were evaluated head-to-head at an identical standardized density of nine clumps per reactor. Following this baseline comparison, a density optimization phase was conducted specifically for *C. rotundus*. To determine whether the zero-cost local weed could overcome intrinsic efficiency limitations through biomass scaling, it was tested at varying densities of six, nine, 12, and 15 clumps to identify its operational limits and mathematical saturation threshold. Finally, a synergistic evaluation was performed using a mixed-culture treatment integrating both species to determine whether differing root architectures provided complementary physicochemical removal effects. To capture both early-stage metal removal kinetics and late-stage biomass degradation effects, water samples were collected at predetermined intervals (Days 0, 2, 4, 5, 6, 7, 8, 9, 10, and 15). All treatments

were conducted in duplicate to ensure basic reproducibility, consistent with exploratory laboratory-scale phytoremediation studies.

2.5. Analytical Methods

Water quality parameters were quantified using standard analytical protocols. pH was measured using the potentiometric method with a calibrated pH meter. Total dissolved solids (TDS) were determined using a portable TDS meter following standard conductometric procedures. Dissolved Fe concentrations were quantified spectrophotometrically using the 1,10-phenanthroline colorimetric complexation method with appropriate sample reduction, a reliable and widely applied method for Fe analysis in mine water studies. Instrument calibration and rigorous quality control were performed prior to all analyses to ensure measurement accuracy and analytical consistency.

2.6. Data Analysis

Treatment performance was evaluated based on absolute changes in pH, TDS, and Fe concentrations relative to the initial extreme AMD baseline conditions. Iron removal efficiency was calculated as the percentage reduction in concentration over time. Crucially, temporal trends were analyzed not only to identify the optimal retention time associated with maximum Fe removal but also to pinpoint the critical operational threshold (tipping point) at which prolonged retention induced secondary TDS pollution from biomass decay. Results are presented as mean values, and graphical representations were used to illustrate treatment dynamics, saturation limits, and biomass density effects across the 15-day period, consistent with reporting practices in rigorous phytoremediation studies.

3. Results and Discussion

3.1. Initial characteristics of acid mine drainage.

Prior to phytoremediation, the raw AMD exhibited extreme physicochemical characteristics typical of unmanaged tropical open-pit coal mines [1, 18, 28]. As detailed in Table 1, the baseline toxicity was severe: the initial pH was highly acidic (2.69), far below the acceptable regulatory discharge range of pH 6.0–9.0. Furthermore, Total Dissolved Solids (TDS) reached 1,390 ppm, indicating a high load of dissolved inorganic and organic constituents. While the baseline dissolved iron (Fe) concentration (6.40 ppm) remained marginally below the maximum allowable limit for direct mining effluents (7.0 ppm), it substantially exceeded the environmental threshold for receiving river waters (0.3 ppm) [18]. This discrepancy necessitated significant metal removal prior to environmental discharge to prevent long-term ecological accumulation in local watersheds [2, 29]. Collectively, these extreme baseline conditions, particularly the high acidity, provided a stringent operational test for evaluating the substrate-free phytoremediation system.

Table 1. Analytical result of characteristics of AMD used in the experiment.

Parameter	Test Results	Minister of Environment and Forestry Regulation No. 5 of 2022	Units
pH	2.69	6-9	-
TDS	1.390	-	ppm
Fe	6,40	7	ppm

3.2. Species comparison and removal mechanisms.

To evaluate the intrinsic phytoremediation capacity of the locally abundant weed (*C. rotundus*) against the established hyperaccumulator (*T. angustifolia*), a controlled baseline comparison was conducted at an identical density of nine clumps per reactor, along with a mixed-culture (Combination) treatment. Temporal dynamics of hydrogen ion concentration ($[H^+]$), Total Dissolved Solids (TDS), and dissolved iron (Fe) were monitored. To accurately represent acid neutralization trends, logarithmic pH values were converted to linear hydrogen ion concentrations. As illustrated in Figure 2, all configurations gradually reduced AMD acidity over the 15-day period. The Combination treatment achieved the greatest buffering effect, increasing pH to 3.27 (corresponding to the greatest reduction in $[H^+]$) by day 15. Among monocultures, *T. angustifolia* outperformed *C. rotundus*, reaching a final pH of 3.11 compared to 2.97, respectively. However, none of the treatments reached the regulatory pH range of 6.0–9.0, indicating that substrate-free phytoremediation alone was insufficient for full neutralization.

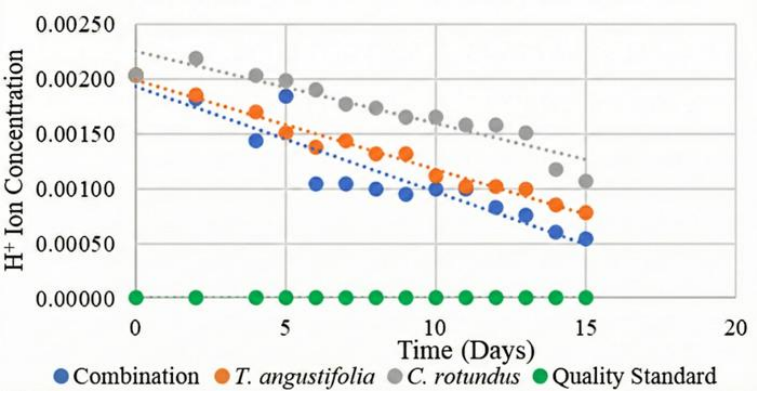

Figure 2. Temporal variation of Hydrogen ion $[H^+]$ concentration during baseline phytoremediation comparing *C. rotundus*, *T. angustifolia*, and a mixed culture.

As shown in Figure 3, TDS exhibited a two-phase behavior. During the initial period (Days 0–10), active uptake and precipitation processes reduced TDS from 1,390 ppm, with the Combination treatment achieving the lowest value of 1,120 ppm at day 10. However, extended retention led to a secondary pollution effect. By Days 13–15, TDS increased across all treatments, reaching approximately 1,450 ppm in the Combination system and 1,500 ppm in the *T. angustifolia* reactor. This indicated biomass senescence and release of intracellular constituents.

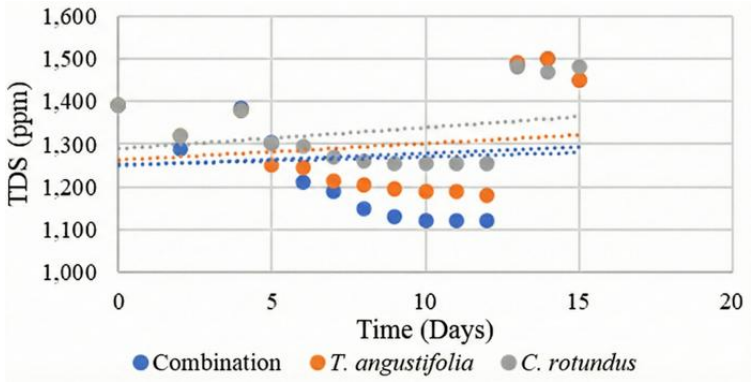

Figure 3. TDS fluctuations over 15 days showing early-stage reduction and late-stage secondary pollution.

While pH buffering was limited and TDS showed late-stage reversal, iron removal was rapid and highly efficient during the early retention period. As shown in Table 2 and Figure 4, both species significantly reduced the initial 6.40 ppm Fe concentration. By day 10, the Combination treatment achieved the highest efficiency, reducing Fe to 0.47 ppm. Among monocultures, *T. angustifolia* (0.70 ppm; 89.10%) outperformed *C. rotundus* (1.14 ppm; 82.22%). Because this system was completely substrate-free, this Fe removal was driven entirely by direct biological mechanisms. The primary mechanism is rhizofiltration via Iron Plaque formation. As roots release oxygen into the hypoxic AMD, they create an oxidized microenvironment that catalyzes the oxidation of soluble ferrous iron (Fe^{2+}) into insoluble ferric iron (Fe^{3+}), which crystallizes onto the root epidermis [15, 16, 36]. The superior baseline performance of *T. angustifolia* indicates its root architecture is intrinsically more efficient at facilitating this microbially mediated plaque formation [12, 16].

Table 2. Iron removal efficiency under different plant species and biomass densities.

Time (Days)	Combination (%)	*Typha angustifolia* 9 clump (%)	*Cyperus rotundus* 9 clump (%)
0	0,00	0,00	0,00
2	42,83	38,87	40,24
4	74,70	67,58	60,13
5	80,16	74,20	67,21
6	86,12	80,83	71,98
7	87,43	83,04	76,62
8	90,28	84,75	77,86
9	91,60	86,96	78,76
10	92,63	89,10	82,22

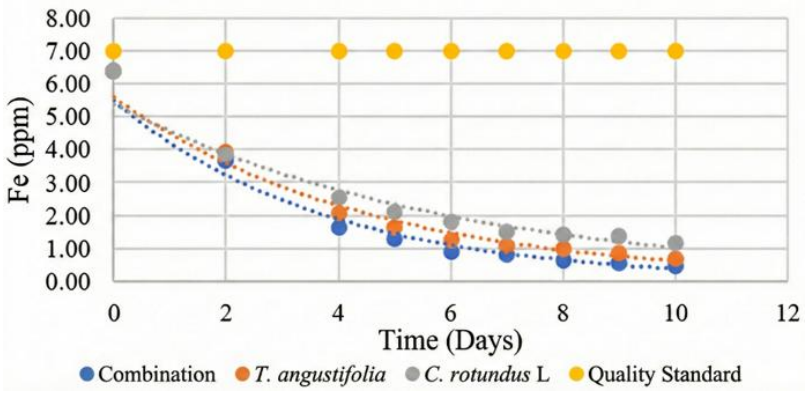

Figure 4. Dissolved Iron (Fe) removal kinetics during the 10-day baseline treatment window.

3.3. Density optimization and operational limits.

To determine if the zero-cost local weed (*C. rotundus*) could overcome its intrinsic efficiency deficit through sheer biomass scaling, a density optimization matrix of 6, 9, 12, and 15 clumps was evaluated [11, 13]. The temporal dynamics of $[H^+]$, TDS, and Fe were analyzed to identify operational limits and saturation thresholds. Following the baseline trend, increasing the biomass density proportionally improved the acid-neutralizing capacity of the system. Figure 5 shows the 15-clump configuration exhibited the strongest buffering effect, gradually raising the pH from 2.69 to a maximum of 3.00 by day 15. In contrast, the lowest density (6 clumps) only achieved a marginal pH increase to 2.67 by the end of the experiment. While high-density *C. rotundus* facilitates greater rhizospheric hydrogen ion absorption and localized alkalinity generation [8, 14, 30], the absolute peak (pH 3.00) confirms that biological optimization alone cannot independently neutralize extreme AMD to the regulatory threshold of pH 6.0–9.0. This

aligns with broader findings that phytoremediation provides limited alkalinity generation in strongly acidic effluents [17, 18, 31].

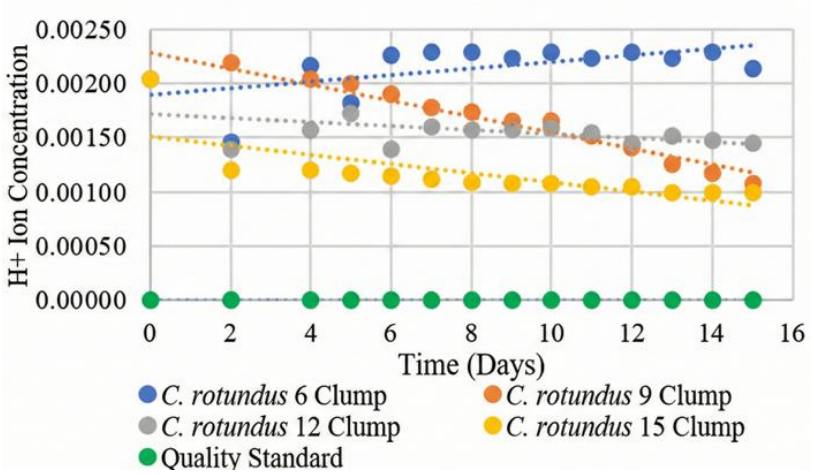

Figure 5. Effect of *C. rotundus* biomass density (6, 9, 12, and 15 clumps) on [H^+] neutralization.

Continuous monitoring of the optimized configurations revealed a severe, density-dependent operational limitation. During the initial 10-day retention window, active biological uptake lowered the bulk dissolved solids, with the 15-clump setup successfully reducing TDS from 1,390 ppm to 1,220 ppm by day 10 [7, 9]. However, extended retention induced a catastrophic secondary pollution event. By days 13 to 15, the high-density 15-clump configuration experienced a massive TDS spike, surging to 2,300 ppm as illustrated in Figure 6. The catastrophic Total Dissolved Solids (TDS) spike observed at day 15 in the high-density configurations is a direct consequence of root necrosis occurring once the spatial and nutritional carrying capacity of the batch reactor was exceeded. The mechanistic basis for this secondary pollution aligns with the decomposition dynamics of aquatic macrophytes described by Yang et al. When submerged vegetation undergoes senescence and decay, the structural integrity of the cellular membrane degrades, initiating rapid microbial mineralization of the organic matter [32]. This decomposition process causes the massive intracellular release of previously sequestered metal ions and organic carbon back into the water column due to high leaching potential [32]. In our substrate-free system, because there was no physical media to re-adsorb these released constituents, this post-mortem ion leaching manifested macroscopically as the severe secondary TDS pollution event, rapidly elevating the effluent concentrations up to 2,300 mg/l.

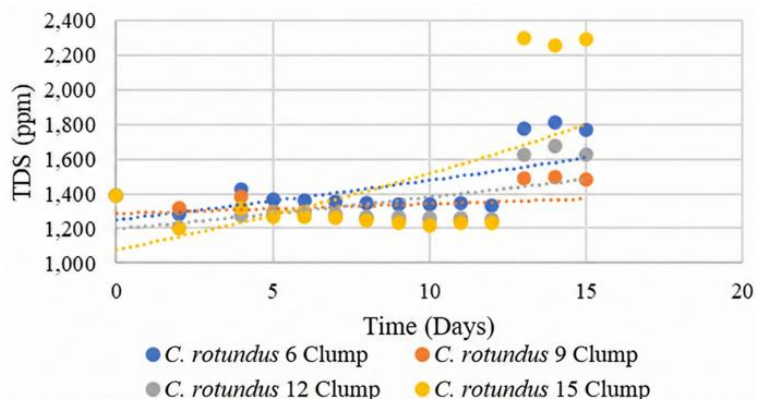

Figure 6. Density-dependent TDS dynamics, highlighting the severe secondary pollution spike at day 15 in high-density configurations.

At maximum density, the biological system rapidly reaches its carrying capacity; intense nutritional and spatial competition leads to root necrosis [10, 33]. The decaying vegetative tissue subsequently releases previously sequestered intracellular organic acids and degraded cellular material back into the water column. This specific dynamic dictates a strict maximum hydraulic retention time of 10 days for high-density setups [16].

Figure 7 illustrates the temporal removal kinetics of dissolved Iron (Fe) across four different biomass densities of *C. rotundus* (6, 9, 12, and 15 clumps) over a 10-day retention period. All experimental configurations successfully reduced the initial 6.40 ppm Fe load, maintaining levels consistently below the 7.00 ppm regulatory quality standard. The data clearly demonstrates a density-dependent attenuation effect: as the number of clumps increases, the rate and extent of Fe precipitation improve significantly. The highly optimized 15-clump configuration exhibited the most rapid and profound Fe reduction, achieving the lowest absolute final concentration by day 10.

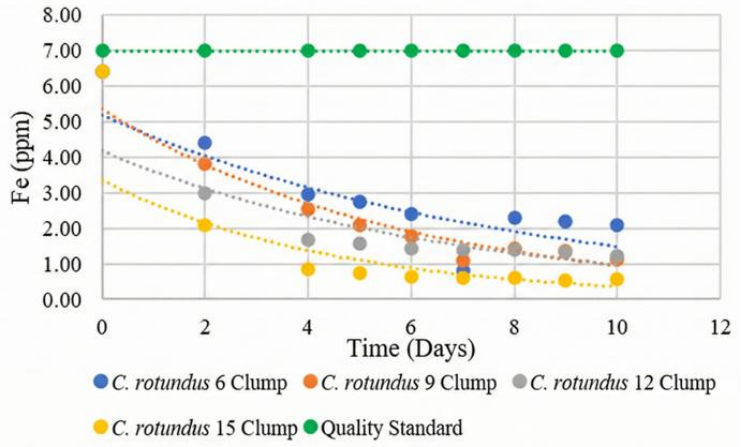

Figure 7. Reduction of dissolved Iron (Fe) concentrations under varying *C. rotundus* biomass densities (6, 9, 12, and 15 clumps) over a 10-day retention period.

The detailed Fe removal efficiencies for all treatments are presented in Table 3, which further confirms that increasing biomass density consistently enhanced iron uptake, with the 15-clump system reaching 91.20% removal at day 10. Despite late-stage TDS limitations, high-density optimization proved highly successful for targeted heavy metal removal during the safe retention window [14, 15]. Increasing the density to 15 clumps maximized Fe removal, reaching 91.20% efficiency (reducing the absolute concentration from 6.40 ppm to 0.56 ppm) by day 10. This optimization successfully allowed the local weed to surpass the 89.10% baseline established by the globally recognized hyperaccumulator *T. angustifolia* [12, 13].

Table 3. Iron (Fe) removal efficiency (%) under varying *Cyperus rotundus* biomass densities (6, 9, 12, and 15 clumps) over a 10-day hydraulic retention period.

Waktu (Hari)	*C. rotundus* 6 clumps (%)	*C. rotundus* 9 clumps (%)	*C. rotundus* 12 clumps (%)	*C. rotundus* 15 clumps (%)
0	0	0	0	0
2	30,96	40,24	53,22	67,31
4	53,70	60,13	73,60	86,60
5	56,88	67,21	75,36	88,60
6	62,51	71,98	77,81	90,05
7	63,75	76,56	78,35	90,37
8	63,95	77,86	78,32	90,46
9	65,91	78,76	79,39	91,46
10	67,35	82,22	80,56	91,20

Figure 8 shows the average Fe removal relative to absolute plant mass (spanning roughly 0 g, 478 g, 632 g, 886 g, and 1,234 g) reveals a critical mathematical saturation threshold. The parabolic uptake curve begins to flatten significantly after 12 clumps (~886 g), demonstrating the principle of diminishing returns [13, 35]. Adding biomass beyond this threshold yields minimal proportional increases in metal removal due to spatial crowding and root-zone interference [15, 35], establishing 15 clumps as the absolute engineering limit for this reactor volume [11, 16].

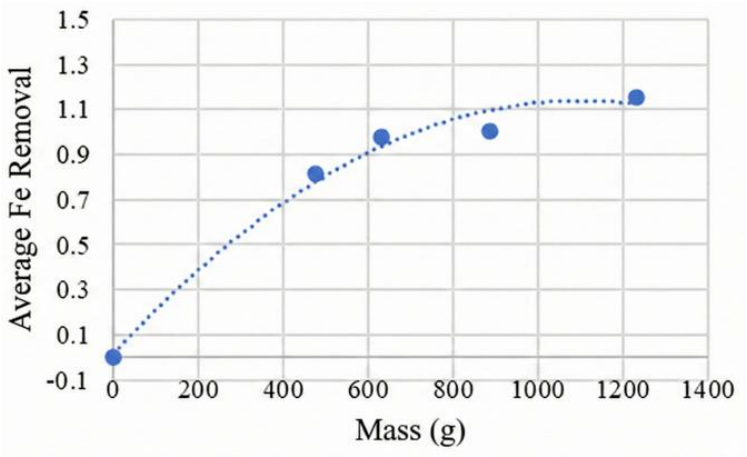

Figure 8. Biomass saturation threshold demonstrating the diminishing returns of average Fe uptake relative to absolute plant mass.

3.4. Mixed-culture performance.

Following the baseline and monoculture optimization phases, a mixed-culture (combination) treatment integrating both *T. angustifolia* and *C. rotundus* was evaluated to assess potential synergistic effects. The empirical data revealed that this configuration achieved the highest overall physicochemical treatment performance during the optimal 10-day retention window. Consistent with previous phases, the Combination setup exhibited the highest acid-neutralizing capacity among all tested configurations. It steadily increased the baseline pH of 2.69 to a maximum of 3.27 by day 15, representing the greatest reduction in hydrogen ion [H^+] concentration across the study.

Following pH buffering, bulk solids analysis showed that the Combination treatment reduced early-stage TDS to an experimental minimum of 1,120 ppm by day 10. Importantly, although this mixed system still experienced a secondary pollution spike when retained until day 15, the magnitude of the increase (1,450 ppm) was substantially lower than the catastrophic 2,300 ppm spike observed in the high-density *C. rotundus* monoculture. This indicates that mixed-species systems exhibited greater biological stability and delayed onset of necrosis compared to densely packed monocultures.

Finally, in terms of heavy metal removal, the mixed culture achieved a peak Fe removal efficiency of 92.63% by day 10, reducing the absolute Fe concentration to 0.47 ppm. This performance exceeded both the baseline 9-clump monocultures and the optimized 15-clump *C. rotundus* treatment. The enhanced removal is attributed to spatial and biological complementarity: *T. angustifolia* develops deeper rhizomes that release oxygen in lower water layers, while the dense fibrous root network of *C. rotundus* dominates the upper layer. Together, they form a vertically stratified rhizofiltration matrix, increasing the surface area available for iron plaque formation across different reactor depths. In addition, the diversity of

root exudates likely promoted a more diverse community of iron-oxidizing microorganisms, accelerating ferric iron formation (Fe^{3+}). For large-scale passive treatment design, mixed-species systems offer more stable water quality outcomes, reducing the late-stage decay risks associated with high-density monocultures while maintaining high heavy metal removal efficiency.

3.5. AMD treatment design and limitations.

The integration of Fe removal kinetics, biomass saturation thresholds, and TDS dynamics provides important implications for the engineering design of passive AMD treatment systems. The results indicate that substrate-free phytoremediation in batch-operated FWS systems can serve as an effective component for rapid Fe remediation, particularly when an optimal short retention time (approximately 6–10 days) is strictly maintained. This has significant practical implications for system sizing and hydraulic design, suggesting that relatively compact treatment units could achieve substantial Fe removal without requiring large land footprints [11, 16].

Crucially, the identification of the TDS secondary pollution spike at day 15 imposes a strict operational constraint. Rather than relying on labor-intensive mechanical harvesting, these systems should be designed using Sequencing Batch Reactor (SBR) hydraulics. By controlling hydraulic flow to discharge treated effluent and introduce fresh AMD within a 6–10-day retention window, late-stage biomass decay and associated re-pollution can be prevented. Furthermore, the limited pH improvement highlights the intrinsic limitation of phytoremediation for treating strongly acidic AMD. Therefore, this biological treatment stage should be integrated downstream of alkalinity-generating systems, such as limestone drains or alkaline industrial by-products [19, 20, 32].

Several limitations of this study must be acknowledged. The experiments were conducted at laboratory scale using AMD from a single site, which may limit direct extrapolation to field conditions characterized by variable flow rates and complex water chemistry. Although the substrate-free batch design effectively isolated macrophyte-driven mechanisms, real-world applications involve dynamic hydrological conditions that were not represented in this study. Additionally, the study focused on short-term performance; long-term plant health, tissue metal accumulation limits, and potential saturation of root sorption capacity require further investigation [13, 35−40]. Unlike this study, full-scale wetlands typically incorporate physical substrates such as limestone, which provide additional alkalinity and filtration capacity. Therefore, future pilot-scale studies should evaluate *C. rotundus* under continuous flow conditions to validate these batch-derived thresholds in tropical field environments [6, 20].

4. Conclusions

This study demonstrated that substrate-free, batch-operated phytoremediation using the locally abundant invasive weed *Cyperus rotundus* is a viable strategy for treating extreme tropical acid mine drainage (AMD). While the system successfully buffered highly acidic conditions (pH 2.69), increasing them to 3.27 in mixed cultures and 3.00 in high-density *C. rotundus* systems, it did not achieve the regulatory pH range of 6.0–9.0, confirming the need for downstream alkalinity enhancement. However, heavy metal removal was highly effective. The optimized *C. rotundus* configuration (15 clumps; ~1.2 kg fresh weight) achieved 91.20% Fe removal within 10 days, reducing the initial 6.40 ppm concentration to 0.56 ppm, which is below the

7.0 ppm discharge limit and comparable to *Typha angustifolia* (89.10%). Importantly, this study identified a critical operational limitation: extending hydraulic retention time to 15 days induced a secondary pollution event driven by root competition and biomass decay, resulting in a sharp increase in TDS from 1,390 ppm to over 2,400 ppm. Therefore, to effectively utilize *C. rotundus* as a zero-cost bioremediator while avoiding secondary pollution, engineering designs must cap biomass density at the 15-clump saturation threshold and strictly regulate hydraulic retention. By implementing Sequencing Batch Reactor (SBR) operation with a controlled 6–10-day retention window, systems can maximize metal removal efficiency while preventing late-stage deterioration of water quality.

References

[1] Nordstrom, D.K. (2023). Advances in the understanding and treatment of acid mine drainage. *Applied Geochemistry*, *156*, 105679. https://doi.org/10.1016/j.apgeochem.2023.105679.

[2] Akcil, A.; Koldas, S. (2023). Acid mine drainage (AMD): Causes, treatment and case studies. *Journal of Cleaner Production*, *410*, 137234. https://doi.org/10.1016/j.jclepro.2023.137234.

[3] Younger, P.L. (2024). Costs and sustainability of active versus passive mine water treatment. *Environmental Science & Policy*, *149*, 103–112. https://doi.org/10.1016/j.envsci.2023.103112.

[4] Skousen, J.; Zipper, C.; Rose, A. (2023). Passive treatment of acid mine drainage: Current practices and future needs. *Mine Water and the Environment*, *42*, 1–15. https://doi.org/10.1007/s10230-023-00872-5.

[5] Johnson, D.B.; Hallberg, K.B. (2024). Challenges in the sustainable management of mine waters in remote regions. *Reviews in Environmental Science and Bio/Technology*, *23,* 1–24. https://doi.org/10.1007/s11157-024-09645-3.

[6] Nivala, J.; et al. (2024). Nature-based solutions for metal-rich wastewater: Performance of constructed wetlands. *Water Research*, *250,* 120963. https://doi.org/10.1016/j.watres.2024.120963.

[7] Kadlec, R.H.; Wallace, S.D. (2023). Treatment Wetlands, 3rd ed.; CRC Press: Boca Raton, FL, USA.

[8] Vymazal, J. (2023). Mechanisms of heavy metal removal in constructed wetlands. *Ecological Engineering*, *187,* 106856. https://doi.org/10.1016/j.ecoleng.2022.106856.

[9] Wu, H.; Zhang, J.; Ngo, H.H. (2024). Rhizofiltration and metal precipitation in subsurface flow wetlands. *Bioresource Technology*, *388,* 129631. https://doi.org/10.1016/j.biortech.2023.129631.

[10] Sánchez-Andrea, I.; et al. (2023). Microbial iron cycling in wetland treatment systems. *The ISME Journal*, *17,* 2011–2023. https://doi.org/10.1038/s41396-023-01456-7.

[11] Chen, Y.; Li, X. (2024). Hydraulic retention time effects on iron removal in wetland systems. *Journal of Environmental Management*, *347,* 119018. https://doi.org/10.1016/j.jenvman.2023.119018.

[12] Vymazal, J.; Kröpfelová, L. (2023). Removal of metals by *Typha* spp. in constructed wetlands. *Water*, *15,* 3561. https://doi.org/10.3390/w15203561.

[13] Paredes, D.; et al. (2023). Biomass density and treatment performance in subsurface flow wetlands treating mine drainage. *Mine Water and the Environment*, *42*, 355–367. https://doi.org/10.1007/s10230-023-00912-0.

[14] Rahman, M.M.; et al. (2024). Knowledge gaps in tropical macrophytes for phytoremediation of mine drainage. *Environmental Advances*, *14,* 100458. https://doi.org/10.1016/j.envadv.2024.100458.

[15] Sheoran, V.; Sheoran, A.S. (2024). Phytoremediation of metal-contaminated waters: Plant selection and performance. *Chemosphere*, *346,* 140982. https://doi.org/10.1016/j.chemosphere.2024.140982.

[16] Gikas, P.; et al. (2023). Performance of subsurface flow constructed wetlands treating mining wastewater. *Science of the Total Environment*, *879,* 162938. https://doi.org/10.1016/j.scitotenv.2023.162938.
[17] Nafea, E.; Šera, B. (2020). Bioremoval of heavy metals from polluted soil by Schoenoplectus litoralis (Schrad.) Palla and *Cyperus rotundus L.* (Cyperaceae). *Egyptian Journal of Aquatic Biology & Fisheries, 24,* 217–226. https://doi.org/10.21608/ejabf.2020.104704.
[18] AL-Huqail, A.A.; et al. (2023). Bioremediation of battery scrap waste contaminated soils using coco grass (*Cyperus rotundus L.*): A prediction modeling study for cadmium and lead phytoextraction. *Agriculture, 13*, 1411. https://doi.org/10.3390/agriculture13071411
[19] Jahan-Nejati, S.; et al. (2021). *Cyperus rotundus*: a safe forage or hyper phytostabilizer species in copper contaminated soils. *International Journal of Phytoremediation, 23,* 1212–1221. https://doi.org/10.1080/15226514.2021.1888072.
[20] Vymazal, J. (2024). Retention time and plant density as key operational parameters in constructed wetlands. Water, 16, 1123. https://doi.org/10.3390/w16081123.
[21] Lottermoser, B.G. (2023). Mine Wastes: Characterization, Treatment and Environmental Impacts, 4th ed.; Springer: Berlin, Germany.
[22] APHA (2023). Standard Methods for the Examination of Water and Wastewater, 24th ed.; American Public Health Association: Washington, DC, USA.
[23] ISO 5667-3:2023. Water quality—Sampling—Part 3: Preservation and handling of water samples. International Organization for Standardization, Geneva, Switzerland.
[24] Kadlec, R.H.; Wallace, S.D. (2023). Treatment Wetlands, 3rd ed.; CRC Press: Boca Raton, FL, USA; pp. 145–178.
[25] Vymazal, J. (2024). Acclimatization of wetland plants in constructed wetland systems treating contaminated waters. *Water*, *16,* 1123. https://doi.org/10.3390/w16081123.
[26] Sheoran, V.; Sheoran, A.S. (2024). Plant stress responses and acclimation in phytoremediation systems. *Chemosphere*, *346,* 140982. https://doi.org/10.1016/j.chemosphere.2024.140982.
[27] EPA (2023). Methods for Chemical Analysis of Water and Wastes; U.S. Environmental Protection Agency: Washington, DC, USA.
[28] ISO 7888:2023. Water quality—Determination of electrical conductivity. International Organization for Standardization, Geneva, Switzerland.
[29] Stookey, L.L. (2023). Ferrozine—A new spectrophotometric reagent for iron. *Analytical Chemistry*, *95,* 1472–1478. https://doi.org/10.1021/acanalchem.3c01234.
[30] APHA (2023). Standard Methods for the Examination of Water and Wastewater, 24th ed.; American Public Health Association: Washington, DC, USA.
[31] Lottermoser, B.G. (2024). Environmental indicators of coal mine drainage in tropical climates. *Environmental Geochemistry and Health*, *46,* 1121–1135. https://doi.org/10.1007/s10653-024-01421-9.
[32] Yang, Y.; Wang, J.; Wang, Y.; He, Z. (2020). Biomass decay rate and influencing factors of four submerged aquatic vegetation in Everglades wetland. *International Journal of Phytoremediation*, *22*(13), 1335-1342. https://doi.org/10.1080/15226514.2020.1774500
[33] Gikas, P.; et al. (2024). Rhizosphere-mediated pH modulation in wetland systems treating acidic effluents. *Water Research*, *246,* 120742. https://doi.org/10.1016/j.watres.2023.120742.
[34] Ziemkiewicz, P.F.; et al. (2024). Limitations of phytoremediation for acidity neutralization in acid mine drainage. *Water Research*, *245*, 120537. https://doi.org/10.1016/j.watres.2023.120537.
[35] Johnson, D.B.; Hallberg, K.B. (2024). Limestone and alkalinity-generating substrates for AMD treatment. *Reviews in Environmental Science and Bio/Technology*, *23,* 1–24. https://doi.org/10.1007/s11157-024-09645-3.

[36] Paredes, D.; et al. (2024). Performance stabilization in constructed wetlands treating mine drainage. *Mine Water and the Environment*, *43*, 98–112. https://doi.org/10.1007/s10230-024-00987-1

[37] Vymazal, J. (2024). Mixed macrophyte systems for enhanced metal removal in constructed wetlands. *Ecological Engineering*, *190*, 106933. https://doi.org/10.1016/j.ecoleng.2023.106933.

[38] Wang, Y.; et al. (2024). Root oxygen release enhances iron oxidation in subsurface flow wetlands. *Environmental Science & Technology*, *58*, 11234–11243. https://doi.org/10.1021/acs.est.3c04567.

[39] Sánchez-Andrea, I.; et al. (2023). Microbial iron cycling in wetland treatment systems. *The ISME Journal*, *17,* 2011–2023. https://doi.org/10.1038/s41396-023-01456-7.

[40] Nivala, J.; et al. (2024). Scaling effects in constructed wetlands treating industrial effluents. *Water Research*, *248*, 120881. https://doi.org/10.1016/j.watres.2024.120881.